American Genetic Association

Journal of Heredity, 2021, 417–429
doi:10.1093/jhered/esab014
Special Issue Article
Advance Access publication April 22, 2021

OXFORD

Special Issue Article

Feather Gene Expression Elucidates the Developmental Basis of Plumage Iridescence in African Starlings

Dustin R. Rubenstein, André Corvelo, Matthew D. MacManes, Rafael Maia, Giuseppe Narzisi, Anastasia Rousaki, Peter Vandenabeele, Matthew D. Shawkey, and Joseph Solomon

From the Department of Ecology, Evolution and Environmental Biology, Columbia University, New York, NY 10027 (Rubenstein, Maia, and Solomon); Center for Integrative Animal Behavior, Columbia University, New York, NY 10027 (Rubenstein); New York Genome Center, New York, NY 10013 (Corvelo and Narzisi); Department of Molecular, Cellular and Biomedical Sciences, University of New Hampshire, Durham, NH 03824 (MacManes); Raman Spectroscopy Research Group, Department of Chemistry, Ghent University, Krigslaan 281, S12, 9000 Ghent, Belgium (Rousaki and Vandenabeele); Archaeometry Research Group, Department of Archaeology, Ghent University, Sint-Pietersnieuwstraat 35, B-9000, Ghent, Belgium (Vandenabeele); and Evolution and Optics of Nanostructures Group, Department of Biology, Ghent University, Ghent, Belgium (Shawkey).

Address correspondence to D. R. Rubenstein at the address above, or e-mail: dr2497@columbia.edu.

Received October 29, 2020; First decision February 2, 2021; Accepted March 19, 2021.

Corresponding Editor: Bridgett vonHoldt

Abstract

Iridescence is widespread in the living world, occurring in organisms as diverse as bacteria, plants, and animals. Yet, compared to pigment-based forms of coloration, we know surprisingly little about the developmental and molecular bases of the structural colors that give rise to iridescence. Birds display a rich diversity of iridescent structural colors that are produced in feathers by the arrangement of melanin-containing organelles called melanosomes into nanoscale configurations, but how these often unusually shaped melanosomes form, or how they are arranged into highly organized nanostructures, remains largely unknown. Here, we use functional genomics to explore the developmental basis of iridescent plumage using superb starlings (*Lamprotornis superbus*), which produce both iridescent blue and non-iridescent red feathers. Through morphological and chemical analyses, we confirm that hollow, flattened melanosomes in iridescent feathers are eumelanin-based, whereas melanosomes in non-iridescent feathers are solid and amorphous, suggesting that high pheomelanin content underlies red coloration. Intriguingly, the nanoscale arrangement of melanosomes within the barbules was surprisingly similar between feather types. After creating a new genome assembly, we use transcriptomics to show that non-iridescent feather development is associated with genes related to pigmentation, metabolism, and mitochondrial function, suggesting non-iridescent feathers are more energetically expensive to produce than iridescent feathers. However, iridescent feather development is associated with genes related to structural and cellular organization, suggesting that, while nanostructures themselves may passively assemble, barbules and melanosomes may require active organization to give them their shape. Together, our analyses suggest that iridescent feathers form through a combination of passive self-assembly and active processes.

Graphical Abstract

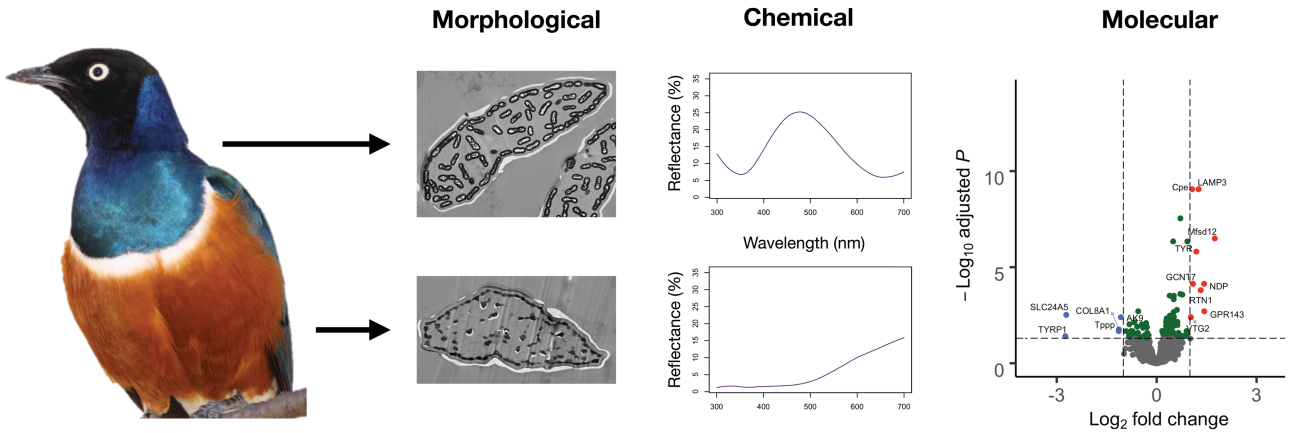

Subject Area: Molecular Adaptation and Selection
Key words: color evolution, structural color, pigmentation, pheomelanin, eumelanin, melanosome, transcriptomics

Colors are multifunctional components of the animal phenotype that are critical to both reproduction (e.g., mate choice) and survival (e.g., camouflage, thermoregulation) (Hill and McGraw 2006). Color can be produced by selective absorption of light by pigments such as melanins and carotenoids, or by light scattering by nanostructural arrangements of materials with varying refractive indices (Prum 2006; Doucet and Meadows 2009). One type of structural color is iridescence (or change in color with viewing or lighting angle), which is found in a variety of organisms ranging from flowers to insects to cephalopods to birds (Doucet and Meadows 2009; Williams et al. 2019). Birds in particular have a rich diversity of structural colors in their iridescent feathers, produced in most cases by the arrangement of melanin-containing organelles called melanosomes into varying nanoscale configurations (D'Alba and Shawkey 2019). Uniquely to birds, the morphology of these melanosomes can vary from the typical oblate or semi-spherical forms seen in other organisms to flattened, plate-like, and/or hollow forms (Durrer 1970; Prum 2006; Maia et al. 2013; D'Alba and Shawkey 2019). These shapes confer additional flexibility to color production by introducing both sharp optical interfaces between materials (e.g., between melanin and air) (Eliason et al. 2013) and new packing arrangements (Eliason et al. 2020) that can enable color diversification that might not otherwise be possible (Maia et al. 2013, 2016).

Although it is clear that nanostructured arrays of melanin and keratin form in feather barbules following deposition of melanosomes by the melanocytes (D'Alba and Shawkey 2019), surprisingly little is known about the process by which either these optical nanostructures or the modified avian melanosomes that comprise them grow. Shawkey et al. (2015) suggested that hollow cylindrical melanosomes in feathers of the wild turkey (*Meleagris gallopavo)* result from selective loss of pheomelanin cores following their deposition in developing barbules. By contrast, Durrer and Villiger (1967) suggested that hollow, flattened melanosomes in the lesser blue-eared glossy starling *(Lamprotornis chloropterus*) form by deposition of melanin on air bubbles (formed as vesicles in the Golgi field) in pre-melanosomes within the melanocyte itself. Since neither of these studies observed—despite their complex and precise arrangement—any evidence of active placement of melanosomes (e.g., via microtubules) into their proper optically active orientation in the barbule, Maia et al. (2012) proposed that iridescent feathers may form via a self-assembly processes, more specifically depletion-attraction forces (i.e., the Asakura-Oosawa model of attraction forces) (Yodh et al. 2001). Since the strength of these processes increases with concentration of both particles (melanosomes, in this case) and polymer (keratin), increases in either should lead to greater self-assembly (Maia et al. 2012). Accordingly, the production of complex, nanostructured iridescent feathers may be similarly (or even less) energetically expensive as the production of more typical unorganized melanin-based plumage, because nanostructuring is created passively via self-assembly forces, with only a small increase in energy potentially used to produce more keratin and melanin. Moreover, the predominant melanin type may also affect the relative energetic cost of feather production, as some evidence suggests pheomelanin is more costly to produce than eumelanin (Galván 2017).

The few published studies on nanostructural development in birds have thus far relied on purely phenotypic data, and, as far as we are aware, no study has examined patterns of gene expression during development in iridescent plumage (but see Gao et al. 2018). Such data are critical for understanding how iridescent feathers form, as they enable a greater understanding of development at a molecular level and can provide insights into processes that may be hidden or difficult to interpret phenotypically.

Here, we use transcriptomics to explore the molecular basis of plumage development in superb starlings (*Lamprotornis superbus*). The African starlings (Sturnidae) are the only monophyletic avian group to display all 4 of the melanosome morphotypes that have been identified in birds (Durrer 1970; Maia et al. 2013). Although each of the 47 species of African starlings exhibit at least some iridescent plumage, a few species, like the superb starling, produce both iridescent and non-iridescent feathers (Figure 1A), the latter likely to be melanin-based. Birds in this species are sexually monomorphic and males and females produce both plumage types. First, we use morphological and chemical analysis to confirm the mechanism of non-iridescent red coloration in superb starlings, and the chemical nature of melanosomes in iridescent blue feathers, since the morphological basis of this color has been previously described (Maia et al. 2013). Next, to understand the developmental and molecular bases

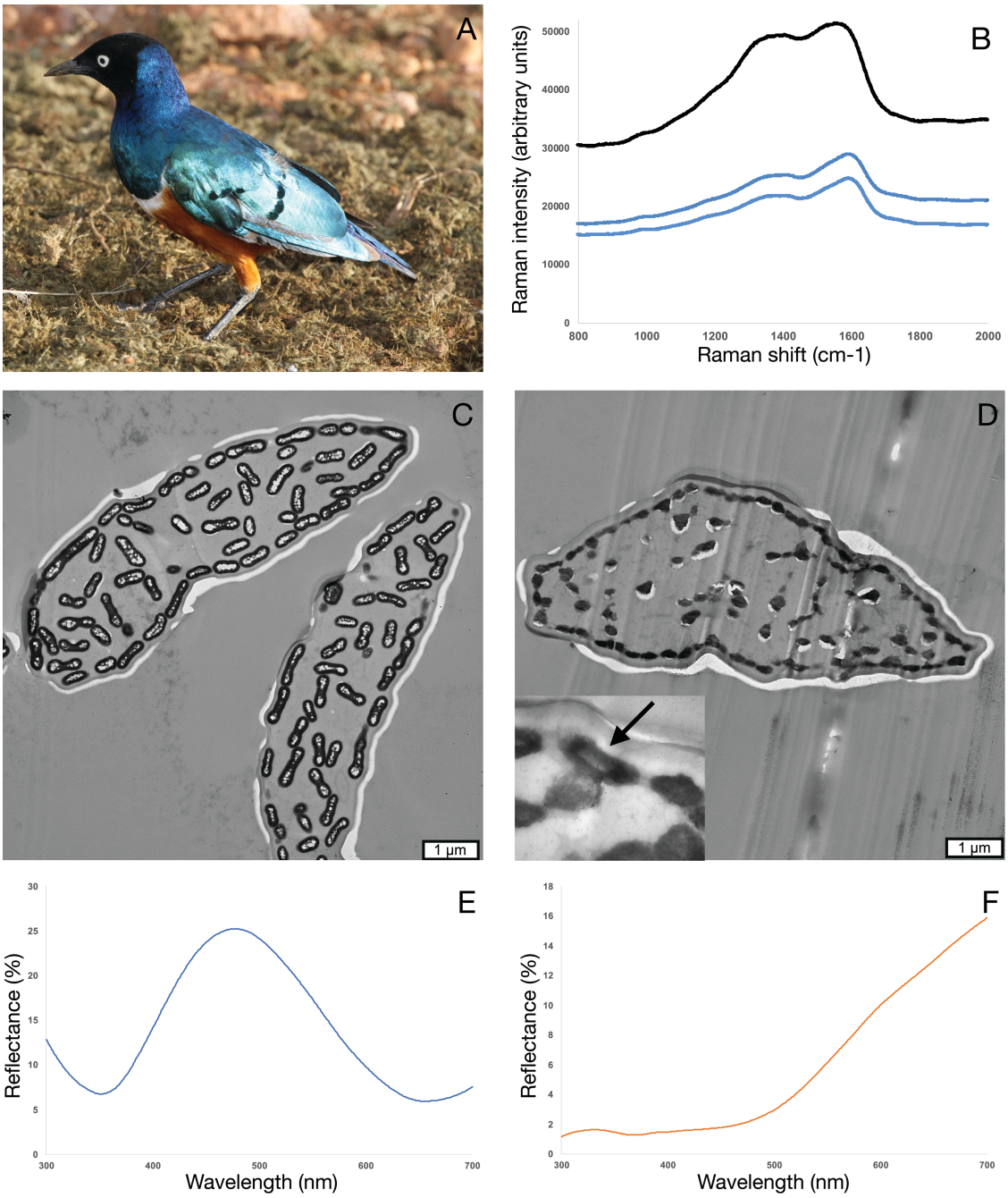

Figure 1. Morphological and chemical differences between iridescent blue and non-iridescent red superb starling feathers. (**A**) Superb starlings have non-iridescent red breast feathers and iridescent blue feathers on their wings, neck, and back. Photo credit: D. Rubenstein. (**B**) Raman spectroscopic data of iridescent blue feathers (see Supplementary Figure S3 for corresponding data from non-iridescent red feathers). The top spectrum is a eumelanin standard and the bottom spectra are samples. Transmission electron microscopy (TEM) images of barbules from (**C**) iridescent and (**D**) non-iridescent feathers. Dark material in both cases is melanin, and grey material is keratin. Inset in D shows a closeup of a melanosomes, with one containing less electron-dense regions (indicated by arrow). Reflectance spectrophotometry of (**E**) iridescent feathers showing a blue peak from the nanostructural arrangement of hollow melanosomes and (**F**) non-iridescent feathers showing a gradually rising reflectance characteristic of pheomelanin-based color.

of iridescence, we assemble and annotate the genome of the superb starling and then compare gene expression during growth of iridescent blue and non-iridescent red feathers. Following the eumelanin shell model that hollow melanosomes form through selective loss of pheomelanin in their core (Shawkey et al. 2015), and the likely presence of pheomelanin in non-iridescent but not iridescent feathers, we predict a greater expression of eumelanin- than pheomelanin-related genes in iridescent blue versus non-iridescent red feathers. Following the depletion-attraction hypothesis (Maia et al. 2012), we predict that iridescent blue feathers will show enhanced expression of keratin- and melanin-production genes, but similar or reduced expression of genes associated with metabolism (since genes related to metabolic function are often upregulated in tissues with high energy demands; Dorji et al. 2020) and with structural components

and cellular organization. This latter prediction would not hold for the Durrer-Villiger model for the formation of hollow melanosomes, which posits high cellular organization activity. Ultimately, our goal is to determine whether functional genomics can provide insights into the developmental basis of iridescent plumage in birds, and thereby test hypotheses about the physical interactions that shape structural color production.

Methods

Sample Collection

Superb starlings were sampled in Kenya in July and August 2017. Although birds appear to molt throughout the year, molt in superb starlings peaks in the period following the long rains breeding season, which typically ends in June in central Kenya (Rubenstein 2016). Birds were captured using pull-string wire traps baited with cornmeal powder and papaya (Rubenstein 2007b). For this study, we used 12 adult sexually mature starlings (5 females and 7 males) that were captured at the Mpala Research Centre (0°17′25.61″ N, 36°53′42.25″ E), Archers Post (0°38′36.72″ N, 37°39′52.68″ E), Nanyuki (0°0′40.07″ N, 37°4′3.36″ E), and Embu (0°32′2.36″ S, 37°27′12.78″ E). All research was approved by the Institutional Animal Care and Use Committees at Columbia University, as well as the Kenyan National Commission for Science, Technology, and Innovation, the Kenyan National Environmental Management Authority, the National Museums of Kenya, the Kenya Wildlife Service, and the Mpala Research Centre.

Each of these birds that we used in this study exhibited both molting breast (non-iridescent red) and back feathers (iridescent blue) (Figure 1A). Up to 10 molting pin feathers (including both developing barbs and barbules) per body region were collected from each bird using forceps and submerged in RNA later inside a 1.5 ml Eppendorf tube and immediately frozen at −80°C in a liquid nitrogen dry shipper. Both iridescent blue and non-iridescent red feathers were collected from the same birds at similar stages of molt as much as possible in the field, and only those at similar stages (determined visually by their size and appearance) were chosen for RNA extraction and sequencing. Samples were transported on dry ice to the United States and stored at −80°C until extraction. We also collected a blood sample from each bird in 2% SDS Queen's Lysis Buffer (Seutin et al. 1991) and transported to the United States at room temperature. DNA for molecular sexing was isolated from blood using a Qiagen DNeasy Blood & Tissue Kit and sex was determined using PCR primers (Griffiths et al. 1998) that have been confirmed previously in this species (Rubenstein 2007a; Pollack and Rubenstein 2015; Weinman et al. 2015).

Electron Microscopy

We used standard techniques to compare the nanoscale morphology of fully developed iridescent blue and non-iridescent red feathers from some of the same individuals from which developing pin feathers were sampled. We first embedded feathers in Epon (Electron Microscopy Solutions, Hatfield, PA), then stained thin (100 nm) sections in Uranyless/lead citrate, and examined them on a JEOL JEM 1010 (Jeol, Ltd, Tokyo, Japan) transmission electron microscope.

Reflectance Spectrophotometry

We used UV-vis spectrophotometry to characterize the reflectance of fully developed feathers from some of the same individuals from which developing pin feathers were sampled. We measured whole feather specular reflectance between 300 and 700 nm using an Avantes AvaSpec-2048 spectrometer and an AvaLight-XE pulsed xenon light source, relative to a WS-2 white reflectance standard (Avantes Inc., Boulder, CO). The spectral data of 3 overlapping feathers were collected at a 90° angle of incidence for the light and probe using AvaSoft v7.2. We analyzed the reflectance spectra using pavo v2.0 in R (Maia et al. 2019).

Micro-Raman Spectroscopy

To identify the pigments present in these feathers, we used Raman spectroscopy, a molecular, surface sensitive technique able to identify both organic and inorganic compounds. Feather barbules were measured with a Bruker Optics Senterra dispersive Raman spectrometer coupled with 2 lasers, a diode laser at 785 mm and a green Nd:YAG at 532 nm. The system is attached to a thermoelectrically cooled (TEC) charged-couple detector (CCD) cooled down to −65°C. The iridescent blue feathers were analyzed with the 532 nm laser, within the 60–2750 cm^{-1} spectral region and with a ~3–5 cm^{-1} spectral resolution. The 50× magnification objective of the Raman microscope was used (NA = 0.75) with a spot size of 4 μm. The acquisition time was set to 60 accumulations of 30 s while the laser power was kept sufficiently low in order to avoid thermal alterations (0.1 mW). No sufficient structural information was acquired from the measurements conducted on the non-iridescent red feathers, even when greater measuring times were employed (120 accumulations of 60 s measured with a 785 nm laser and 100× magnification objective, NA = 0.9, resulting in a 2 μm spot size/spectral resolution at ~9–18 cm^{-1} and laser power at 0.2 mW) or when different experimental conditions or different laser wavelengths (785 and 532 nm) were used. We used eumelanin from squid ink sacs (Sigma-Aldrich, St. Louis, MO) as a standard.

Reference Genome and Transcriptome Sequencing

DNA for the reference genome was extracted using a Qiagen DNeasy Blood & Tissue Kit from liver tissue obtained from one female individual (SS15) captured at the Mpala Research Centre, Kenya in April 2008. Elutions were quantified with a Nanodrop, and samples were sent to the New York Genome Center for library preparation and sequencing. Two Illumina paired end libraries, with 200 and 400 bp of average insert size, were constructed using the Illumina TruSeq kit. These 2 libraries were sequenced on the Illumina HiSeq 2500 sequencing platform (2 × 125 bp), generating 244 and 176 M read pairs, respectively. Extracted DNA was also used as input to create 2 mate pair libraries, utilizing the Illumina Nextera Mate Pair Library Prep Kit v1. Size selection of tagmented and strand displaced DNA fragments was carried out on a Blue Pippin (Sage Science, Beverly, MA) to select 2 sets of fragments, with lengths distributed between 3 and 5 kbp and between 5 and 8 kb. Size selected fragments were then circularized and processed to produce 2 final mate pair libraries that were sequenced on the Illumina HiSeq 2500 sequencing platform (2 × 125 bp), producing 187 and 174 M read pairs, respectively.

Total RNA for the reference transcriptome was extracted from spleen tissue obtained from the same individual (SS15) using a Qiagen RNeasy Tissue Kit. As described previously (Weinman et al. 2015), this sample was sent to The University of Texas at Austin Genome Sequencing and Analysis Facility for TruSeq cDNA library prep with Epicentre Ribo-Zero rRNA depletion, and sequenced on a HiSeq 2000, which produced 138 M 2 x 101 bp read pairs.

Reference Genome Assembly

DNA library read quality was assessed with FastQC v0.11.2 (Andrews 2010). Mate pair data were processed with NextClip v1.3.1 (Leggett et al. 2014). All short reads were error-corrected using the Bloom filter-based error correction tool BLESS v0.17 (Heo et al. 2014) and then quality- and adapter-trimmed with Trimmomatic v0.32 (Bolger et al. 2014). Processed reads were finally de novo assembled using ALLPATHS-LG v49414 (Gnerre et al. 2011) to produce a high-quality draft genome reference. Gene completeness was evaluated using BUSCO v3.0.2 (Simão et al. 2015) against the aves_odb9 dataset.

Reference Transcriptome Assembly

cDNA library read quality was assessed with FastQC v0.11.2. Reads were then error corrected using Lighter v1.0.5 (Song et al. 2014) and trimmed with Trimmomatic v0.32 (Bolger et al. 2014). Processed reads were digital-normalized to 50 median *K*-mer abundance with khmer v1.3 (Crusoe et al. 2015) and then assembled with Trinity v2.02 (Grabherr et al. 2011). TransDecoder v2.0.1 (Grabherr et al. 2011) was used to identify ORFs of 100 amino acids or longer. The resulting candidate peptides were homology-searched against the UniProt database (Consortium 2015) using BLASTP (Altschul et al. 1990) with an e-value cutoff of $1e^{-5}$ and searched for Pfam protein domains (Finn et al. 2014). BLASTP and Pfam domain hits were then retained along with coding region predictions.

Gene and Repeat Annotation

Gene annotation was carried out using the pipeline MAKER v2.31.8 (Cantarel et al. 2008). The Trinity-assembled transcripts were used as EST evidence, and protein evidence consisted of UniProt BLAST protein homologies from multiple avian species. In a first run, Augustus v3.0 (Stanke et al. 2006) was trained with CEGMA v2.5 (Parra et al. 2007) and TransDecoder outputs, and SNAP (Korf 2004) ran with a Hidden Markov Model derived from the CEGMA GFF output converted to ZFF. MAKER was then re-run with SNAP retrained on the initial MAKER model GFF output that was also converted to ZFF. RepeatMasker v4.0.5 (Smit et al. 2013-2015) was used with default pipeline parameters to annotate interspersed repeats. Barrnap v0.4.2 (http://github.com/tseemann/barrnap) was used to predict ribosomal RNA, which was then added to the MAKER annotation.

Gene Expression

Each developing pin feather was excised, disrupted on a Qiagen TissueLyzer II, and then extracted for total RNA using a Qiagen RNeasy Tissue Kit. We added Qiagen Reagent DX to each sample prior to disruption to reduce foaming and improve extraction efficiency. For each individual, the RNA from 3 feathers was pooled for analysis. RNA integrity number equivalent (RIN^e) was quantified on an Agilent 4200 TapeStation and concentration determined using a Qubit 3.0 Fluorometer (Thermo Fisher Scientific). All samples had a $RIN^e > 9.4$ and sufficient concentration for sequencing. Extracted RNA was sent to The University of Texas at Austin Genome Sequencing and Analysis Facility for TagSeq library preparation and sequencing on the Illumina HiSeq 2500 platform. TagSeq is a cost-effective mRNA 3′ end focused alternative to RNA-Seq for generating read count data suitable for differential expression analysis (Meyer et al. 2011; Lohman et al. 2016). The target range for each sample was 3–5 M reads, with a range of 4.1–4.5 M reads passing per sample.

Raw TagSeq reads were concatenated, then adapter and quality trimmed, and removed of PCR duplicates using a script created by tagseq_trim_launch.pl from https://github.com/z0on/tag-based_RNAseq. The trimmed reads were aligned to our *Lamprotornis superbus* genome reference using STAR 2.6.1a (Dobin et al. 2013) with—quantMode GeneCounts option to produce counts for annotated gene features while mapping. Ultimately, STAR produced 83% to 90% uniquely mapped reads per sample (mean = 88%) while outputting read counts per gene.

Differential Expression and Gene Network Analysis

Gene counts were prefiltered for genes where fewer than 6 samples had more than 4 normalized counts (median ratios), corresponding to roughly one count per million raw reads for at least a quarter of the sample set. This filtering of genes with low expression profiles was intended to remove bias from *P*-value histograms and potential noise for later Weighted Correlation Network Analysis (WGCNA) module construction (Langfelder and Horvath 2008). We performed differential expression analysis using DESeq2 v1.26.0 (Love et al. 2014) in R (Team 2019), with the design including feather color (iridescent and non-iridescent) and sex (male and female) as factors, and independent filtering. We used the Benjamini-Hochberg procedure to adjust the false discovery rate and calculate P_{adj} (Benjamini and Hochberg 1995). Although we initially included an interaction term for color and sex, this interaction contained no significant genes (indicating that the iridescent blue versus non-iridescent red marginal differences were consistent between males and females), and therefore we excluded the interaction term from our final models.

A *P*-value histogram for DESeq2 iridescent blue versus non-iridescent red feather results showed weighting towards zero, with a distribution neither hill- nor u-shaped, indicating that the estimated variance of the null distribution was neither too high nor too low. Additionally, a PCA plot of variance-stabilizing transformed counts had distinct clustering for iridescent and non-iridescent feather samples on the PC2 axis and by sex along the PC1 axis (Supplementary Figure S1). This separation in clustering for PC2 indicated a strong enough color trait signal for network analysis to be informative with 12 samples per color group.

Dispersion and log2 fold changes were visualized with the plotMA function, with and without the *apeglm* shrinkage estimator (Zhu et al. 2018) and the *EnhancedVolcano* package (Blighe et al. 2019). Using DESeq2's contrast argument, we generated results tables for iridescent versus non-iridescent feathers, male versus female, and iridescent versus non-iridescent feathers by sex, to explore the color condition effect on each group. *P*-value histograms were assessed for each table, along with gene count plots. A PCA plot of variance-stabilizing transformed count data grouped by factor was used to examine their effects. Heatmaps were created for the top 10 upregulated iridescent and non-iridescent genes using pheatmap v1.0.12 (Kolde 2019).

In addition to looking at expression differences in individual genes, we also examined gene networks using WGCNA. The prefiltered read counts from DESeq2 were transformed with DESeq2's variance-stabilizing transformation *vst* function. These transformed counts were used for gene network construction and module identification with WGCNA v1.69 (Langfelder and Horvath 2008, 2012). Based on scale independence and mean connectivity plots of network topology, a soft-threshold power of 7 was

chosen to calculate adjacency with co-expression similarity. We used the signed hybrid network option for the adjacency matrix, as well as the TOMtype and biweight midcorrelation parameters, for co-expression similarity. Following the step-by-step network construction and module detection approach for expression data, we derived a topological overlap matrix (TOM) from the adjacency matrix, and then a dissimilarity matrix from the TOM.

To identify modules (which the software denotes with the names of colors that are unrelated to feather coloration), we used the *hclust* function to create a gene dendrogram. The dynamic tree cut method for dendrogram branch cutting was employed and then compared with further merging of modules based on calculated eigengenes. The resulting merged modules were examined for module-trait association, with feather color as our selected trait converted to a binary variable of 1 = non-iridescent and 0 = iridescent. We created a table with module-trait relationships to visualize the module eigengenes most significantly associated with the color trait, and then calculated gene significance (GS) (i.e., each gene's correlation with the trait) and module membership values (i.e., the correlation of each gene's expression profile to module eigengenes). For those modules significantly correlated with the color trait, we plotted module membership against GS, and we exported a table of all genes sorted by GS and module membership values, grouped by module color.

We used the web-based software package Enrichr (Chen et al. 2013; Kuleshov et al. 2016) on genes in iridescent blue and non-iridescent red upregulated sets, and on gene lists with expression profiles correlated to the module eigengenes from the WGCNA results for those modules associated with the color trait. Enrichr was also used to explore pathway hits in the KEGG 2019 (https://www.genome.jp/kegg/pathway.html), Reactome 2016 (https://reactome.org), BioPlanet 2019 (Huang et al. 2019), and Panther 2016 (Mi et al. 2019) databases. A Fisher's exact test was used to assess input genes and gene-set overlap ($P_{adj} < 0.05$) (Neyman and Pearson 1928).

Results

Feather Morphology and Pigment Analysis

Morphology and chemistry clearly differed between iridescent blue and non-iridescent red feathers (Figure 1). As is typical, iridescent barbules were flattened relative to the rounder non-iridescent barbules (Figure 1C,D). Transmission electron microscopy (TEM) revealed a single layer of air-filled, semi-flattened, and/or peanut-shaped melanosomes around the edge of iridescent feather barbules (Figure 1C). This morphology has been previously described in *Lamprotornis* starlings (Durrer 1970; Maia et al. 2013) and produces metallic iridescent colors through interference. In contrast, melanosomes in non-iridescent feathers were primarily solid (but see inset in Figure 1D and Supplementary Figure S1) and amorphous, suggesting a high pheomelanin content (Jimbow et al. 1983). Although not directly comparable due to differences in interpretation of SEM and TEM images, their ~300–500 nm size is consistent with melanosomes found in brown feathers, that is, "pheomelanosomes" (Li et al. 2012). Additionally, spectral data of iridescent feathers showed a peak around 500 nm (Figure 1E), whereas non-iridescent feathers showed gradually increasing reflectance across the visible spectrum (Figure 1F), characteristic of pheomelanin-based feathers and distinct from the sigmoid shape of red carotenoid-based feathers (Toral et al. 2008) and the near-uniformly low reflectance of eumelanin-based black feathers (Maia et al. 2011; D'Alba et al. 2014).

Raman spectroscopy revealed the likely presence of eumelanin in iridescent blue feathers. Bands at ~1590 and ~1380 cm^{-1} in the spectra from the iridescent feathers were attributed to the presence of eumelanin (Figure 1B). The Raman results were consistent with previously published work where eumelanin was extracted from extant avian feathers and mammalian hair (Galván et al. 2013; Peteya et al. 2016) or measured as synthetic compound (Perna et al. 2013), and with a eumelanin standard (Figure 1B). These results were not consistent with Raman spectra of red carotenoids (Thomas et al. 2014) (red Psittacofulvins are only found in the order *Psittaciformes*). By contrast, spectra obtained from the non-iridescent red feathers gave no valuable information regarding pigmentation (Supplementary Figure S2) (even when several different experimental conditions were used), possibly due to fluorescence from the samples. Although we cannot conclusively confirm that pheomelanin is present in red feathers, we consider it most likely due to the spectrophotometric and morphological data presented above.

Surprisingly, the arrangement of melanosomes in non-iridescent red feathers was similar to that in iridescent blue feathers: in both cases, melanosomes were arranged around the edge of barbules. This arrangement contributes to the production of thin-film interference color in iridescent feathers (Maia et al. 2013) and may produce the glossy sheen observed in non-iridescent feathers (Maia et al. 2012). This similarity implies that both feather types underwent some level of nanostructural organization of melanosomes, and therefore that comparisons of melanosome organization between the two would be uninformative. We therefore limited our interpretations to differences in melanosome and barbule macrostructural morphology, rather than to differences in melanosome organization.

Reference Genome Assembly

We produced a high-quality draft of the *Lamprotornis superbus* genome by combining 2 paired-end and 2 mate-pair short read libraries (see Methods). These were *de novo* assembled in ALLPATHS-LG (Gnerre et al. 2011) to produce a 1.07 Mb genome reference, with a scaffold N50 length of 4.39 Mb and a contig N50 length of 122.55 Kb (Supplementary Table S1). The draft assembly shows a high level of gene-space completeness, with 4674 out of 4915 (95.1%) avian ortholog groups being found in their complete (i.e., full-length) form by BUSCO (Simão et al. 2015), including 4627 of those as single-copy genes. Of 15 209 genes annotated using the MAKER pipeline (Cantarel et al. 2008), 14 846 contained coding sequences (CDSs) and 14 065 annotated homologies; 14 271 were multi-exonic genes, 1144 (7.5%) had unknown function or were pseudogenes, and 781 of these had annotated coding regions for proteins of unknown function.

Differential Gene Expression in Iridescent Blue and Non-iridescent Red Feathers

We examined gene expression in RNA extracted from the molting iridescent blue and non-iridescent red pin feathers collected from the same individuals. TagSeq (Meyer et al. 2011; Lohman et al. 2016) generated 4.1–4.5 million raw reads per sample (n = 12 per group) (Supplementary Appendix 1). Out of 6883 total genes with non-zero read count after prefiltering and 15 209 annotated reference genes for alignments, we found 95 genes upregulated in non-iridescent red feathers and 42 genes upregulated in iridescent blue feathers (at $P_{adj} \leq 0.05$) (Benjamini and Hochberg 1995) (Figure 2A; Supplementary Appendix 2). Heatmaps for the top 10 genes upregulated in iridescent

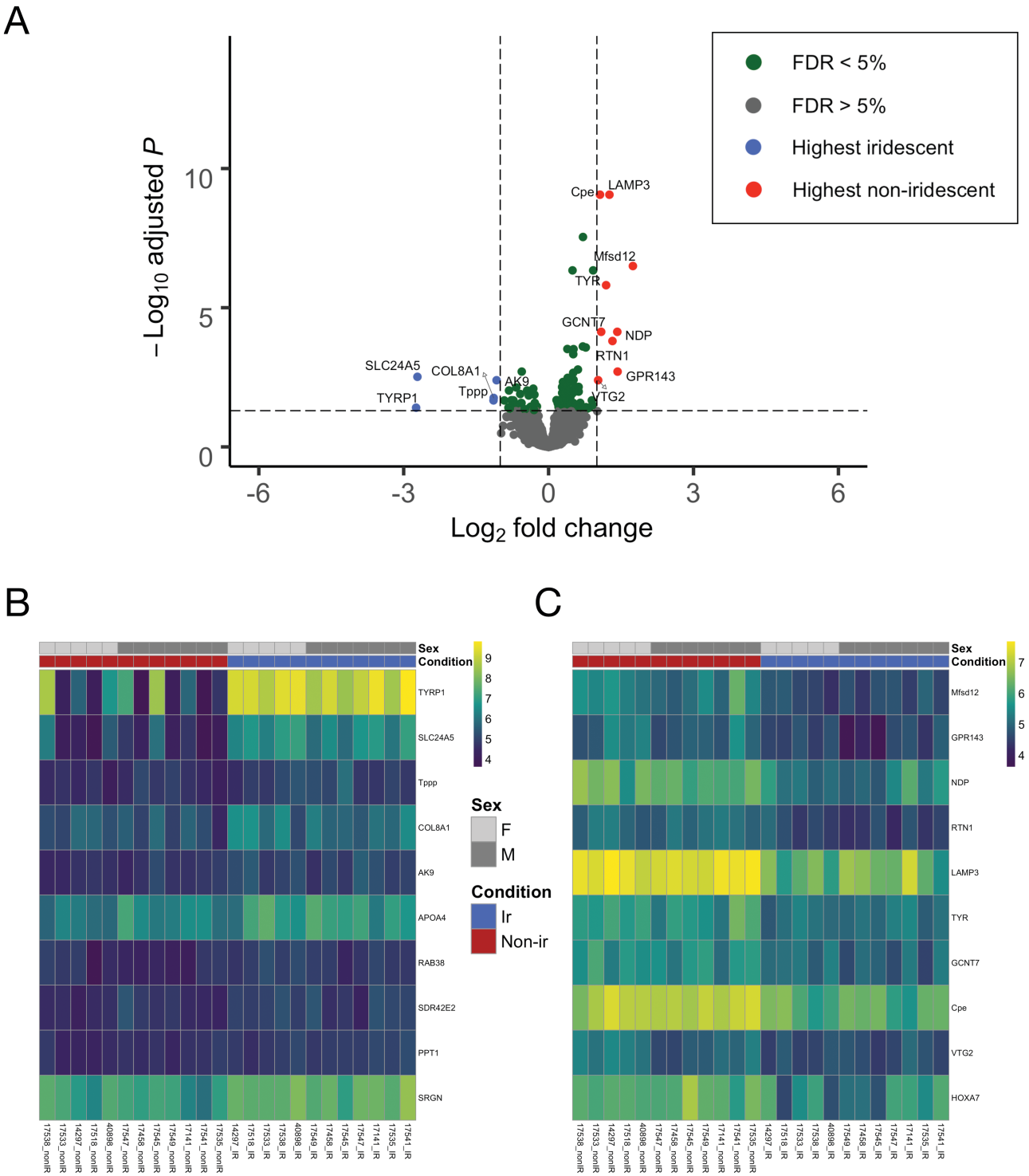

Figure 2. Gene expression differences in iridescent blue and non-iridescent red superb starling feathers. (**A**) Log_2 fold change by $-Log_{10}$ P_{adj} volcano plot of differentially expressed genes from contrast results of non-iridescent (non-ir) versus iridescent (ir) feather groups (N = 6883 genes after filtering). Genes with both Log_2 fold change > 1.0 and P_{adj} < 0.05 that are upregulated in non-iridescent feathers are labeled and colored red, whereas genes upregulated in iridescent feathers with both Log_2 fold change < −1.0 and P_{adj} < 0.05 are labeled and colored blue. Genes within 1.0/−1.0 Log_2 fold change are colored green. All other gene points are colored gray. Vertical dashed lines indicate Log_2 fold change > 1 and < −1. The horizontal dashed line indicates P_{adj} < 0.05. Heatmaps of variance-stabilizing transformed (VST) counts for the top 10 differentially expressed genes in (**B**) iridescent and (**C**) non-iridescent feather groups. Columns correspond to individual feather samples and sex is noted.

(Figure 2B) and non-iridescent feathers (Figure 2C), respectively, illustrate genes with the highest and most consistent log_2 fold changes across feather groups.

We were particularly interested in genes with known functions relating to pigmentation, metabolism, and structural and cellular organization that differed in expression between iridescent blue

and non-iridescent red feathers. Known pigment-related genes upregulated in non-iridescent feathers included tyrosinase (TYR) and G protein-coupled receptor 143 (GPR143), 2 genes involved in melanin production (Cortese et al. 2005; De Filippo et al. 2017), as well as major facilitator superfamily domain-containing protein 12 (MFSD12), which is associated with higher pigmentation (Crawford et al. 2017), and Norrin precursor (NDP), which is related to pigmentation differences (Vickrey et al. 2018). Known pigment-related genes upregulated in iridescent feathers included tyrosinase-related protein 1 (TYRP1) (Nadeau et al. 2007; Xu et al. 2013) and Ras-related protein (RAB38), which are thought to be involved in TYR sorting (Loftus et al. 2002), as well as sodium/potassium/calcium exchanger 5 (SLC24A5), which is associated in humans and zebra fish with melanosomal changes and mutations for lighter skin pigmentation (Lamason et al. 2005; Crawford et al. 2017). In non-iridescent feathers (but not in iridescent feathers), we also identified a number of genes related to mitochondrial function and oxidative phosphorylation, including the mitochondrial citrate carrier SLC25A1 (Edvardson et al. 2013), subunits of the NADH:Ubiquinone Oxidoreductase complex (NDUFB3, NDUFB8, and NDUFB10) (Nakama et al. 2012), Ubiquinol-Cytochrome C Reductase complex (UQCRQ and UQCRFS1) (Garcia et al. 2008; Vempati et al. 2008), and mitochondrial ATP synthase (ATP5F1 and ATP5J2) (Wolf 2016), as well as MRPL/MRPS genes encoding for mitochondrial ribosomal proteins (Sylvester et al. 2004; Hill et al. 2019). Interestingly, the majority of significant terms found by the software package Enrichr (Chen et al. 2013) were for processes related to mitochondrial function (see Supplementary Appendix 2 for more details). Finally, we also found a number of structural genes upregulated in iridescent feathers (but not in non-iridescent feathers), including tubulin polymerization-promoting protein (TPPP) (Lehotzky et al. 2010) and collagen alpha-1(VIII) chain (COL8A1), a key component in extracellular matrix (Shuttleworth 1197). The only significant Gene Ontology (GO) term found during the analysis of iridescent feathers was focal adhesion (Supplementary Appendix 2), which represents mechanosensory machines that integrate spatiotemporal cues to affect critical decision-making process at the cellular level (Geiger and Yamada 2011). We note that the iridescent feather upregulated results differ by sex more than the non-iridescent upregulated results, but small sample sizes limit our ability to further explore sex differences in developmental gene expression in this sexually monochromatic species.

Gene Network Analysis

Next, we used WGCNA (Langfelder and Horvath 2008) to examine gene networks associated with differential expression between iridescent blue and non-iridescent red feathers. Our analysis identified 14 modules after merging based on eigengenes (Table 1). Three modules (Black, Turquoise, and Greenyellow) consisted of genes with expression profiles and module eigengene direction associated with the non-iridescent portion of the color trait, whereas 3 modules (Magenta, Blue, and Grey60) were associated with the iridescent portion of the color trait (Supplementary Appendix 2). Gene set enrichment analysis with the Enrichr software package found GO terms and pathway results for the trait-associated WGCNA modules using lists of genes with expression profiles correlated to the module eigengenes (at > 0.4 and > 0.5 GS thresholds). For the non-iridescent feather eigengene direction for the color trait, the Black module generated GO Cellular Component terms related only to pigmentation (e.g., lysosome, melanosome, and pigment granule), whereas the Turquoise and Greenyellow modules included a larger number of genes involved in metabolism and mitochondrial function (e.g., mitochondrion, mitochondrial components, and mitochondrial translation), as well as ribosomal function (e.g., ribosome, ribosome assembly, translation, transcription, and rRNA processing) (see Supplementary Appendix 2 for more detail). For the iridescent feather eigengene direction for color trait, both the Magenta and Blue modules generated genes associated with structural organization (e.g., microtubule organizing center, tubulin binding, centrosome, spindle assembly, chromatin, axon guidance, focal adhesions, proteoglycans, and cadherin binding), whereas the Grey60 module produced no significant gene hits (see Supplementary Appendix 2 for more detail). Additionally, the blue module had a number of genes inferred to be related to keratin structure, as has been suggested for colored feathers—including iridescent colors—from other gene expressions studies of birds (Gao et al. 2018).

To examine the overlap of differentially expressed genes with WGCNA module genes, we compared positive (non-iridescent red feather upregulated) and negative (iridescent blue feather upregulated) Wald statistic DESeq2 genes (Love et al. 2014) (at $P_{adj} < 0.1$) with the 3 modules associated with each eigengene direction (Supplementary Appendix 2). The lookup for each module consisted of those genes with gene trait significance at $P < 0.05$, or a GS correlation of approximately 0.40 and above (Langfelder and Horvath 2008). We found that 87% of the iridescent upregulated genes and 89% for the non-iridescent upregulated genes from DESeq2 were found in the corresponding WGCNA modules (Figure 3), indicating high overlap in our 2 approaches. Together, these 2 approaches suggest that developing non-iridescent red feathers were associated more with genes for pigmentation and metabolic function, whereas developing iridescent

Table 1. WGCNA constructed 14 modules (indicated by color names that are unrelated to feather coloration) after merging based on eigengenes and one module for unassigned genes

Module	Number of genes assigned to module	Correlation of module eigengenes	*P*-value
Black	**534**	**0.62**	**0.001**
Turquoise	**1107**	**0.54**	**0.007**
Greenyellow	**228**	**0.43**	**0.04**
Lightgreen	121	0.20	0.3
Cyan	304	0.11	0.6
Green	664	0.057	0.8
Lightcyan	150	0.029	0.9
Magenta	**633**	**–0.66**	**<0.0001**
Blue	**1217**	**–0.46**	**0.02**
Grey60	**131**	**–0.40**	**0.05**
Midnightblue	177	–0.20	0.3
Tan	224	–0.15	0.5
Brown	609	–0.083	0.7
Pink	289	–0.0054	1.0
Grey (unassigned genes)	495	–0.065	0.8

Positive correlation coefficients indicate modules associated with the non-iridescent red portion of the color trait, whereas negative correlation coefficients indicate modules associated with the iridescent blue portion of the color trait. Bolding indicates modules with significant *P*-values (<0.05) and large correlation coefficients.

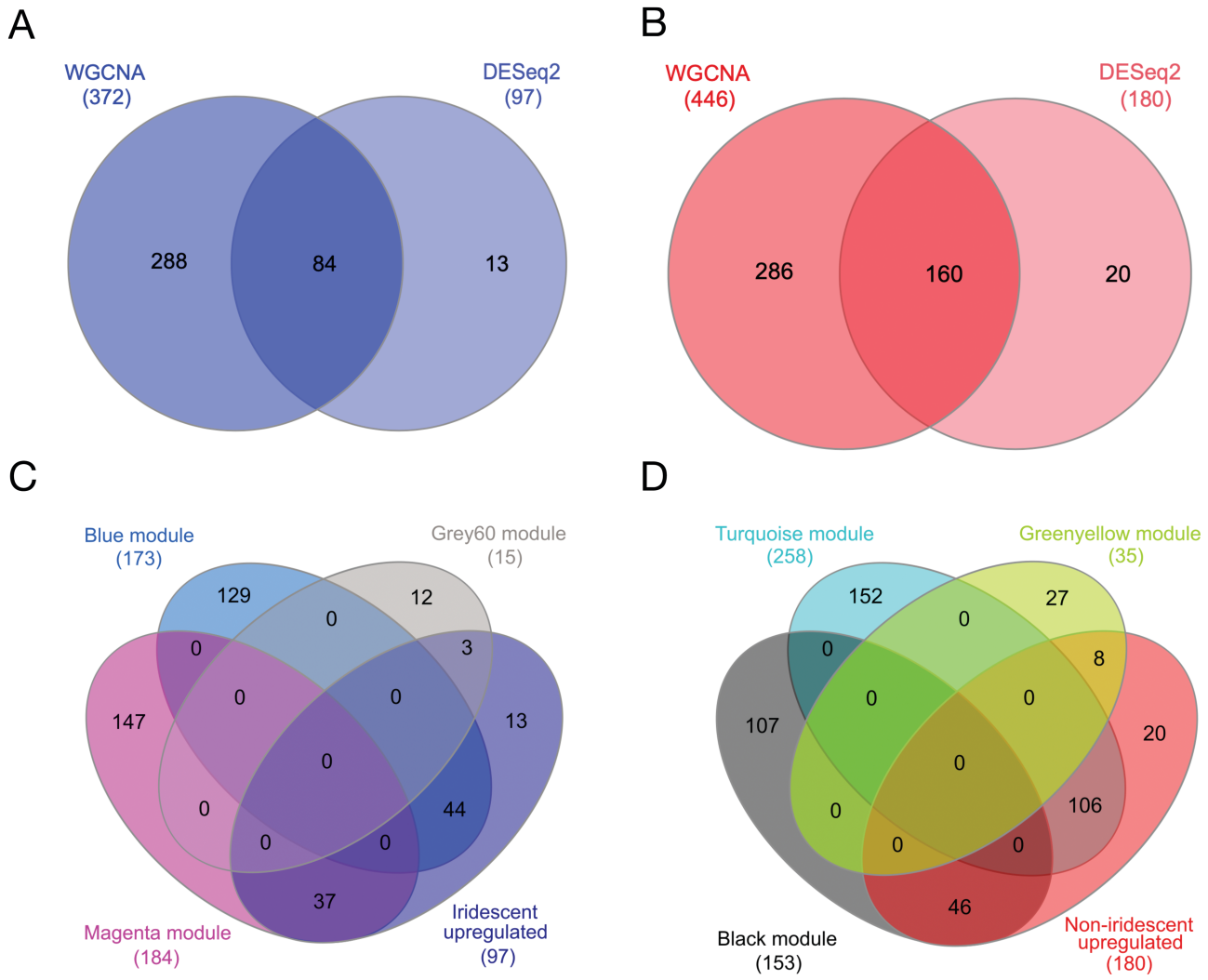

Figure 3. Overlap of WGCNA color trait-associated modules in (**A**) iridescent blue direction (GS < 0.05) and DESeq2 iridescent feather upregulated genes at P_{adj} < 0.1 and (**B**) non-iridescent red direction (GS < 0.05) and DESeq2 non-iridescent feather upregulated genes at P_{adj} < 0. Overlap of genes within individual WGCNA modules on (**C**) iridescent upregulated and (**D**) non-iridescent upregulated genes. The colors in C and D refer to module names generated by the software and are unrelated to feather coloration.

blue feathers were associated more with genes for structural and cellular organization.

Discussion

Although iridescent colors are widespread in organisms as diverse as bacteria, plants, and animals, we know surprisingly little about the developmental and molecular bases of the structural colors that give rise to iridescence, particularly compared to pigment-based colors (Hubbard et al. 2010; Toews et al. 2017). To begin to explore the molecular basis of plumage development, we used superb starlings because they produce both iridescent blue plumage and non-iridescent red coloration that is presumably melanin-based. In addition to morphological and chemical analysis, we compared gene expression in iridescent and non-iridescent feathers, as has been done previously for pheasants with differently colored and pigmented feathers (Gao et al. 2018). First, we confirmed, using morphological and chemical analysis, that non-iridescent red coloration in superb starlings is indeed melanin-based and is produced differently than iridescent coloration. We found that non-iridescent feathers 1) contained mostly solid, amorphous melanosomes suggestive of high pheomelanin content that is consistent with melanin-based coloration (Jimbow et al. 1983) and 2) gradually increased in reflectance across the visible spectrum, characteristic of pheomelanin-based feathers (D'Alba et al. 2014) and distinct from the sigmoid shape of red carotenoid-based feathers (Toral et al. 2008). By contrast, iridescent feathers consisted of a single layer of air-filled, semi-flattened, and/or peanut-shaped eumelanosomes around the edge of barbules that produces metallic iridescent colors in *Lamprotornis* starlings through thin-film interference (Durrer 1970; Maia et al. 2013). Intriguingly, pheomelanosomes were localized around the edge of non-iridescent feather barbules, similarly to those in iridescent feathers (Figure 1C,D), although without the thicker outer keratin layer associated with a shiny appearance in feathers (Maia et al. 2012). Thus, iridescent blue and non-iridescent red feathers differed in melanosome and barbule shape, but exhibited a surprisingly similar pattern of melanosome structuring within the barbule. This means that at least some of the differences in gene expression are likely related

to melanosome and barbule shape, and not to nanostructuring (i.e., melanosome organization), although it is possible that melanosome shape/size and barbule shape also contribute to pattern formation by self-assembly, as has been proposed previously (Maia et al. 2012).

Not only are iridescent blue and non-iridescent red feathers produced by different forms of melanin (eumelanin and pheomelanin, respectively), they also show different expression patterns in known pigmentation genes. Our result supports the previous suggestion that, since structural colors have a pigment layer, the same genes that affect the underlying pigments are likely to affect structural color traits (Hubbard et al. 2010). Non-iridescent feathers were associated with greater expression of genes involved in increased melanin production and pigmentation (TYR, GPR143, MFSD12, and NDP) (Cortese et al. 2005; Crawford et al. 2017; De Filippo et al. 2017; Vickrey et al. 2018), whereas iridescent feathers were associated with greater expression of genes associated with reduced melanin production and pigmentation (RAB38 and SLC24A5) (Loftus et al. 2002; Lamason et al. 2005; Crawford et al. 2017). We note, however, that even though they were collected from the same birds at the same time, the iridescent blue and non-iridescent red feathers were collected from different body regions and, despite our best efforts to the contrary, could have been at slightly different developmental stages.

One of the most intriguing patterns was the upregulation of TYR in non-iridescent feathers and the corresponding upregulation of TYRP1 in iridescent feathers. The opposite pattern of expression of these 2 genes was observed in Korean quail (*Coturnix coturnix*) that exhibit a polymorphism in plumage coloration: TYR expression was higher in individuals with black plumage, but TYRP1 expression was higher in individuals with maroon plumage (Xu et al. 2013). The exact function of TYRP1 remains unclear, but it appears to catalyze later steps in eumelanin—but not pheomelanin—production (D'Alba and Shawkey 2019). Similarly, TYRP1 is required for the production of eumelanin but not phaeomelanin in mammals (Zdarsky et al. 1990). Therefore, the difference in its expression may help to explain the presence of eumelanin in iridescent feathers in superb starlings and other birds. The opposite pattern of expression in the Korean quail may be caused by differences in the mechanism of color production (e.g., more eumelanin in the maroon plumage than in the starlings' red plumage), but this requires further investigation. Intriguingly, TYRP1 may also play a role in determining melanosome shape either by itself (Braasch et al. 2019; Li et al. 2019) or via interactions with the protein PMEL (Hellström et al. 2011), suggesting a potential molecular basis for the unusual flattened shape of melanosomes in iridescent feathers. However, despite differential expression of pigmentation genes in both iridescent and non-iridescent feathers, WGCNA only identified a module associated with pigmentation (i.e., lysosomes, melanosomes, and pigment granules) in non-iridescent feathers. Moreover, Pmel (the gene that codes for PMEL) was not differentially expressed in our data. Therefore, despite their more complex morphology, melanosomes in iridescent feathers appear less associated with pigmentation-related gene regulatory networks than non-iridescent feathers. (We note, however, that this could also result from the bulk RNA sequencing approach diluting the signal from the melanocytes.) This expression pattern may help explain why, once evolved, complex hollow melanosomes are rarely lost (Maia et al. 2013), as reverting back to a simpler morphology would require the gain of a more complex gene network. However, this may not be true if the switch is between hollow and solid eumelanosomes, rather than hollow eumelanosomes and pheomelanosomes as we describe here. Further studies examining gene expression patterns in black feathers of superb starlings are needed to disentangle whether the complexity of the gene network of red feathers is due to the chemistry or shape of the melanosome. This also raises the question of why hollow melanosomes, with apparently less well-integrated gene networks involving fewer genes, have not evolved more often in birds.

Although non-iridescent melanosomes were structurally simpler than iridescent melanosomes, non-iridescent feathers were both associated with the expression of twice as many genes as iridescent feathers, and also may be more costly to produce. That is, WGCNA identified 2 modules associated with the non-iridescent portion of the color trait that contained GO terms and pathways related to mitochondrial and ribosomal function. Since genes related to metabolic function are often upregulated in tissues with high energy demands (Dorji et al. 2020), non-iridescent feathers may be more energetically demanding to produce than iridescent feathers, a result consistent with the depletion-attraction hypothesis (Maia et al. 2012). This difference may be driven in part by the potentially higher cost of producing pheomelanin than eumelanin (Galván 2017). In addition, WGCNA identified 2 modules associated with the iridescent portion of the color trait that contained GO terms and pathways related to structural components and cellular organization (e.g., microtubule organizing center, centrosome, and chromatin). This result supports the Durrer-Villiger (1967) model, in which air bubbles in melanosomes are formed via production of vesicles from the Golgi system. Interestingly, the most common Enrichr term from one of the iridescent feather modules was for focal adhesions, protein structures that play a critical role in linking cells to mechanical structures like actin (Geiger and Yamada 2011). However, none of these structural components were seen in images of nanostructural development in a closely related African starling species with similar feather nanomorphology (Durrer and Villiger 1967). Given the nanostructural similarities between iridescent and non-iridescent feathers, the genes in this module are likely associated with the overall shape of the barbule, which is considerably flatter in iridescent than non-iridescent feathers, or with the development of the unusual melanosome shape. This hypothesis is consistent with another gene expression study in birds, which suggested that the expression of adhesion molecules is associated with differences in barbule shape (Chang et al. 2019). Thus, we identify a relationship between the degree of complexity of feather morphology and patterns of gene expression. Non-iridescent red feathers have morphologically simpler melanosomes that involve the expression of more genes during development and more complicated gene networks that are primarily related to metabolism and mitochondrial function. In contrast, iridescent feathers represent more complex physical structures, but may actually be less energetically expensive to produce and involve the expression of fewer genes overall, including those mostly related to structural and cellular organization.

Although our morphological and chemical analysis suggests differences in the form of melanin between iridescent and non-iridescent feathers, we note the limitations of our experimental design because both feather types show a surprisingly similar arrangement of melanosomes. That is, we compared an iridescent, eumelanin-based feather with eumelanosomes clustered around the edge of the barbule to a non-iridescent feather that most likely contains pheomelanin, but that also has melanosomes clustered around the edge of the barbule. Consequently, the differences in gene expression between these feather types likely reflect differences in pigment type (eumelanin vs. pheomelanin), as would be expected in a comparison between any 2 feathers with different kinds of pigments

regardless of whether one was iridescence. However, because of the similarity in melanosome arrangement between the 2 feather types, the differences in gene expression do not directly provide insights into melanosome nanostructuring, which is arguably the most important characteristic separating iridescent feathers from non-iridescent feathers. Superb starlings also have black feathers on their head and mask, which are not glossy and therefore unlikely to show a similar arrangement of melanosomes to red and blue feathers. Although examining patterns of gene expression in these black feathers would have helped address genetic architecture of melanosome nanostructuring, most birds were not molting this plumage when we collected samples.

In summary, we have shown for the first time that the genes and gene networks associated with the development of melanin-based non-structural and structural colors in bird feathers from the same individuals are quite different. Although both types of developing feathers were characterized by the upregulation of known pigmentation genes, phaeomelanin-based non-iridescent red feathers tended to be associated with greater expression of genes involved in increased melanin production and pigmentation, whereas iridescent blue feathers tended to be associated with greater expression of genes associated with reduced melanin production and pigmentation, as well as one gene, TYRP1, that may not only be related to eumelanin production (Zdarsky et al. 1990), but also help explain the derived melanosome shape characteristic of iridescent feathers in starlings and other birds (Durrer and Villiger 1967; Maia et al. 2013). Non-iridescent red feathers were also associated with larger gene networks related to mitochondrial and ribosomal function, suggesting that phaeomelanin-based plumage may be more energetically expensive to produce than iridescent plumage. In contrast, iridescent blue feathers were associated with smaller gene networks related to structural and cellular organization that are likely related to melanosome and/or barbule morphology. Despite the limitations of gene expression studies, this work demonstrates how functional genomics can be used to not only test hypotheses (e.g., depletion-attraction hypothesis (Maia et al. 2012) and the Durrer and Villiger model (Durrer and Villiger 1967; Maia et al. 2013)) about the physical interactions that shape color production, but also generate new hypotheses relating feather morphology to genetic architecture. Ultimately, our morphological, chemical, and molecular analyses support the idea that iridescent feathers may form via an energetically inexpensive self-assembly process, but one that still involves organizing structures.

Supplementary Material

Supplementary data are available at *Journal of Heredity* online.

Funding

This work was supported by the US National Science Foundation (grant numbers IOS-1257530 and IOS-1656098 to D.R.R.), the Simons Foundation Society of Fellows (to R.M.), the Research Foundation–Flanders (FWO-Vlaanderen) (grant numbers 12X1919N to A.R. and G007117N to M.D.S.), the US Air Force Office of Scientific Research (grant number FA9550-1-0447 to M.D.S.), and the Human Frontiers Science Program (grant number RGP0047 to M.D.S.).

Acknowledgments

We are grateful to W. Watetu, S. Guindre-Parker, S. Shah, G. Manyaas, and J. Mosiany for their assistance in the field. J. Podnar provided assistance with the TagSeq.

Data Availability

All sequence data were deposited in NCBI's Sequence Read Archive under BioProject Accessions PRJNA260278, PRJNA666205, and PRJNA666448.

References

Altschul SF, Gish W, Miller W, Myers EW, Lipman DJ. 1990. Basic local alignment search tool. *J Mol Biol*. 215:403–410.

Andrews S. 2010. FastQC: a quality control tool for high throughput sequence data. Babraham Bioinformatics version 0.11.2. Available from: https://www.bioinformatics.babraham.ac.uk/projects/fastqc/.

Benjamini Y, Hochberg Y. 1995. Controlling the false discovery rate: a practical and powerful approach to multiple testing. *J R Stat Soc Series B*. 57:289–300.

Blighe K, Rana S, Lewis M. 2019. EnhancedVolcano: Publication-ready volcano plots with enhanced colouring and labeling. R package version 1.4.0. Available from: https://github.com/kevinblighe/EnhancedVolcano.

Bolger AM, Lohse M, Usadel B. 2014. Trimmomatic: a flexible trimmer for Illumina sequence data. *Bioinformatics*. 30:2114–2120.

Braasch I, Liedtke D, Volff JN, Schartl M. 2019. Pigmentary function and evolution of tyrp1 gene duplicates in fish. *Pigment Cell Melanoma Res*. 22:839–850.

Cantarel BL, Korf I, Robb SM, Parra G, Ross E, Moore B, Holt C, Sánchez Alvarado A, Yandell M. 2008. MAKER: an easy-to-use annotation pipeline designed for emerging model organism genomes. *Genome Res*. 18:188–196.

Chang WL, Wu H, Chiu YK, Wang S, Jiang TX, Luo ZL, Lin YC, Li A, Hsu JT, Huang HL, *et al.* 2019. The making of a flight feather: bio-architectural principles and adaptation. *Cell*. 179:1409–1423.e17.

Chen EY, Tan CM, Kou Y, Duan Q, Wang Z, Meirelles GV, Clark NR, Ma'ayan A. 2013. Enrichr: interactive and collaborative HTML5 gene list enrichment analysis tool. *BMC Bioinformatics*. 14:128.

Consortium UniProt. 2015. UniProt: a hub for protein information. *Nucleic Acids Res*. 43:D204–2012.

Cortese K, Giordano F, Surace EM, Venturi C, Ballabio A, Tacchetti C, Marigo V. 2005. The ocular albinism type 1 (OA1) gene controls melanosome maturation and size. *Invest Ophthalmol Vis Sci*. 46:4358–4364.

Crawford NG, Kelley DE, Hansen MEB, Beltrame MH, Fan S, Biowman SL, Jewett E, Ranciaro A, Thompson S. 2017. Loci associated with skin pigmentation identified in African populations. *Science*. 17:eaan8433.

Crusoe MR, Alameldin HF, Awad S, Boucher E, Caldwell A, Cartwright R, Charbonneau A, Constantinides B, Edvenson G, Fay S, *et al.* 2015. The khmer software package: enabling efficient nucleotide sequence analysis. *F1000Res*. 4:900.

D'Alba L, Shawkey MD. 2019. Melanosomes: biogenesis, properties, and evolution of an ancient organelle. *Physiol Rev*. 99:1–19.

D'Alba L, van Hemert C, Spencer KA, Heidinger BJ, Gill L, Evans NP, Monaghan P, Handel CM, Shawkey MD. 2014. Melanin-based color of plumage: role of condition and of feathers' microstructure. *Integr Comp Biol*. 54:633–644.

De Filippo E, Schiedel AC, Manga P. 2017. Interaction between G-coupled protein receptor 143 and tyrosinase: implications for understanding ocular albinism type-1. *J Investig Dermatol*. 137:457–465.

Dobin A, Davis CA, Schlesinger F, Drenkow J, Zaleski C, Jha S, Batut P, Chaisson M, Gingeras TR. 2013. STAR: ultrafast universal RNA-seq aligner. *Bioinformatics*. 29:15–21.

Dorji J, Vander Jagt CJ, Garner JB, Marett LC, Mason BA, Reich CM, Xiang R, Clark EL, Cocks BG, Chamberlain AJ, *et al.* 2020. Expression of mitochondrial protein genes encoded by nuclear and mitochondrial genomes correlate with energy metabolism in dairy cattle. *BMC Genomics*. 21:720.

Doucet SM, Meadows MG. 2009. Iridescence: a functional perspective. *J R Soc Interface*. 6(Suppl 2):S115–S132.

Durrer H. 1970. Schillerfarben der stare (*Sturnidae*) [Iridescent colors of the starlings (*Sturnidae*)]. *J Ornithol*. 111:133–153.

Durrer H, Villiger W. 1967. Bildung der schillerstruktur beim glanzstar. *Z Zellforsch Mik Ana*. 81:445–456.

Edvardson S, Porcelli V, Jalas C, Soiferman D, Kellner Y, Shaag A, Korman SH, Pierri CL, Scarcia P, Fraenkel ND, *et al.* 2013. Agenesis of corpus callosum and optic nerve hypoplasia due to mutations in SLC25A1 encoding the mitochondrial citrate transporter. *J Med Genet*. 50:240–245.

Eliason CM, Bitton PP, Shawkey MD. 2013. How hollow melanosomes affect iridescent colour production in birds. *Proc Biol Sci*. 280:20131505.

Eliason CM, Maia R, Parra JL, Shawkey MD. 2020. Signal evolution and morphological complexity in hummingbirds (Aves: Trochilidae). *Evolution*. 74:447–458.

Finn RD, Bateman A, Clements J, Coggill P, Eberhardt RY, Eddy SR, Heger A, Hetherington K, Holm L, Mistry J, *et al.* 2014. Pfam: the protein families database. *Nucleic Acids Res*. 42:D222–D230.

Galván I. 2017. Condition-dependence of pheomelanin-based coloration in nuthatches Sitta europaea suggests a detoxifying function: implications for the evolution of juvenile plumage patterns. *Sci Rep*. 7:9138.

Galván I, Jorge A, Solano F, Waka-Matsi K. 2013. Vibrational characterization of phaeomelanin and trichochrome F by Raman spectroscopy. *Spectrochim Acta A Mol Biomol Spectrosc*. 110:55–59.

Gao G, Xu M, Bai C, Yang Y, Li G, Xu J, Wei Z, Min J, Su G, Zhou X, *et al.* 2018. Comparative genomics and transcriptomics of Chrysolophus provide insights into the evolution of complex plumage coloration. *GigaScience*. 7:1–14.

Garcia S, Diaz F, Moraes CT. 2008. A 3′ UTR modification of the mitochondrial rieske iron sulfur protein in mice produces a specific skin pigmentation phenotype. *J Investig Dermatol*. 128:2343–2345.

Geiger B, Yamada KM. 2011. Molecular architecture and function of matrix adhesions. *Cold Spring Harb Perspect Biol*. 3:a005033.

Gnerre S, Maccallum I, Przybylski D, Ribeiro FJ, Burton JN, Walker BJ, Sharpe T, Hall G, Shea TP, Sykes S, *et al.* 2011. High-quality draft assemblies of mammalian genomes from massively parallel sequence data. *Proc Natl Acad Sci U S A*. 108:1513–1518.

Grabherr MG, Haas BJ, Yassour M, Levin JZ, Thompson DA, Amit I, Adiconis X, Fan L, Raychowdhury R, Zeng Q, *et al.* 2011. Full-length transcriptome assembly from RNA-Seq data without a reference genome. *Nat Biotechnol*. 29:644–652.

Griffiths R, Double MC, Orr K, Dawson RJ. 1998. A DNA test to sex most birds. *Mol Ecol*. 7:1071–1075.

Hellström AR, Watt B, Fard SS, Tenza D, Mannström P, Narfström K, Ekesten B, Ito S, Wakamatsu K, Larsson J, *et al.* 2011. Inactivation of Pmel alters melanosome shape but has only a subtle effect on visible pigmentation. *PLoS Genet*. 7:e1002285.

Heo Y, Wu XL, Chen D, Ma J, Hwu WM. 2014. BLESS: bloom filter-based error correction solution for high-throughput sequencing reads. *Bioinformatics*. 30:1354–1362.

Hill GE, Hood WR, Ge Z, Grinter R, Greening C, Johnson JD, Park NR, Taylor HA, Andreasen VA, Powers MJ, *et al.* 2019. Plumage redness signals mitochondrial function in the house finch. *Proc Biol Sci*. 286:20191354.

Hill GE, McGraw KJ. 2006. *Bird coloration: function and evolution*. Cambridge (MA): Harvard University Press.

Huang R, Grishagin I, Wang Y, Zhao T, Greene J, Obenauer JC, Ngan D, Nguyen DT, Guha R, Jadhav A, *et al.* 2019. The NCATS BioPlanet - an integrated platform for exploring the universe of cellular signaling pathways for toxicology, systems biology, and chemical genomics. *Front Pharmacol*. 10:445.

Hubbard JK, Uy JA, Hauber ME, Hoekstra HE, Safran RJ. 2010. Vertebrate pigmentation: from underlying genes to adaptive function. *Trends Genet*. 26:231–239.

Jimbow K, Ishida O, Ito S, Hori Y, Witkop CJ Jr, King RA. 1983. Combined chemical and electron microscopic studies of pheomelanosomes in human red hair. *J Invest Dermatol*. 81:506–511.

Kolde R. 2019. pheatmap: Pretty Heatmaps. R package version 1.0.12. Available from: https://CRAN.R-project.org/package=pheatmap

Korf I. 2004. Gene finding in novel genomes. *BMC Bioinformatics*. 5:59.

Kuleshov MV, Jones MR, Rouillard AD, Fernandez NF, Duan Q, Wang Z, Koplev S, Jenkins SL, Jagodnik KM, Lachmann A, *et al.* 2016. Enrichr: a comprehensive gene set enrichment analysis web server 2016 update. *Nucleic Acids Res*. 44:W90–W97.

Lamason RL, Mohideen MA, Mest JR, Wong AC, Norton HL, Aros MC, Jurynec MJ, Mao X, Humphreville VR, Humbert JE, *et al.* 2005. SLC24A5, a putative cation exchanger, affects pigmentation in zebrafish and humans. *Science*. 310:1782–1786.

Langfelder P, Horvath S. 2008. WGCNA: an R package for weighted correlation network analysis. *BMC Bioinformatics*. 9:559.

Langfelder P, Horvath S. 2012. Fast R functions for robust correlations and hierarchical clustering. *J Stat Softw*. 46:1–17.

Leggett RM, Clavijo BJ, Clissold L, Clark MD, Caccamo M. 2014. NextClip: an analysis and read preparation tool for Nextera Long Mate Pair libraries. *Bioinformatics*. 30:566–568.

Lehotzky A, Lau P, Tokési N, Muja N, Hudson LD, Ovádi J. 2010. Tubulin polymerization-promoting protein (TPPP/p25) is critical for oligodendrocyte differentiation. *Glia*. 58:157–168.

Li J, Bed'hom B, Marthey S, Valade M, Dureux A, Moroldo M, Péchoux C, Coville JL, Gourichon D, Vieaud A, *et al.* 2019. A missense mutation in TYRP1 causes the chocolate plumage color in chicken and alters melanosome structure. *Pigment Cell Melanoma Res*. 32:381–390.

Li Q, Gao KQ, Meng Q, Clarke JA, Shawkey MD, D'Alba L, Pei R, Ellison M, Norell MA, Vinther J. 2012. Reconstruction of Microraptor and the evolution of iridescent plumage. *Science*. 335:1215–1219.

Loftus SK, Larson DM, Baxter LL, Antonellis A, Chen Y, Wu X, Jiang Y, Bittner M, Hammer JA 3rd, Pavan WJ. 2002. Mutation of melanosome protein RAB38 in chocolate mice. *Proc Natl Acad Sci U S A*. 99:4471–4476.

Lohman BK, Weber JN, Bolnick DI. 2016. Evaluation of TagSeq, a reliable low-cost alternative for RNAseq. *Mol Ecol Resour*. 16:1315–1321.

Love MI, Huber W, Anders S. 2014. Moderated estimation of fold change and dispersion for RNA-seq data with DESeq2. *Genome Biol*. 15:550.

Maia R, D'Alba L, Shawkey MD. 2011. What makes a feather shine? A nanostructural basis for glossy black feathers. *Proc R Soc Lond [Biol]*. 278:1973–80.

Maia R, Gruson H, Endler JA, White TE. 2019. pavo2: new tools for the spectral and spatial analysis of colour in R. *Methods Ecol. Evol*. 10:1097–1107.

Maia R, Macedo RH, Shawkey MD. 2012. Self-assembly of iridescent barbules through depletion attraction of melanosomes during keratinization. *J R Soc Interface*. 9:734–743.

Maia R, Rubenstein DR, Shawkey MD. 2013. Key ornamental innovations facilitate diversification in an avian radiation. *Proc Natl Acad Sci U S A*. 110:10687–10692.

Maia R, Rubenstein DR, Shawkey MD. 2016. Selection, constraint, and the evolution of coloration in African starlings. *Evolution*. 70:1064–1079.

Meyer E, Aglyamova GV, Matz MV. 2011. Profiling gene expression responses of coral larvae (*Acropora millepora*) to elevated temperature and settlement inducers using a novel RNA-Seq procedure. *Mol Ecol*. 20:3599–3616.

Mi H, Muruganujan A, Ebert D, Huang X, Thomas PD 2019. PANTHER version 14: more genomes, a new PANTHER GO-slim and improvements in enrichment analysis tools. *Nucleic Acids Res*. 47:D419–426.

Nadeau NJ, Mundy NI, Gourichon D, Minvielle F. 2007. Association of a single-nucleotide substitution in TYRP1 with roux in Japanese quail (*Coturnix japonica*). *Anim Genet*. 38:609–613.

Nakama M, Murakami Y, Tanaka H, Nakata S. 2012. Decrease in nicotinamide adenine dinucleotide dehydrogenase is related to skin pigmentation. *J Cosmet Dermatol*. 11:3–8.

Neyman J, Pearson ES 1928. On the use and interpretation of certain test criteria for purposes of statistical inference. *Biometrika*. 20A:175–240.

Parra G, Bradnam K, Korf I. 2007. CEGMA: a pipeline to accurately annotate core genes in eukaryotic genomes. *Bioinformatics*. 23:1061–1067.

Perna G, Lasalvia M, Gallo C, Quartucci G, Capozzi V. 2013. Vibrational characterization of synthetic eumelanin by means of Raman and Surface Enhanced Raman Scattering. *Open Surf Sci*. 5:1–8.

Peteya J, Clarke JA, Li Q, Gao KQ, Shawkey MD. 2016. The plumage and colouration of an enantiornithine bird from the Early Cretaceous of China. *Paleontology*. 60:55–71.

Pollack LJ, Rubenstein DR. 2015. The fitness consequences of kin-biased dispersal in a cooperatively breeding bird. *Biol Lett*. 11:20150036.

Prum RO. 2006. Physics and evolution of structural colors. In: Hill GE,McGraw KJ, editors. *Bird coloration: volume 1: mechanisms and measurements*. Cambridge (MA): Harvard University Press. p. 295–353.

Rubenstein DR. 2007a. Female extrapair mate choice in a cooperative breeder: trading sex for help and increasing offspring heterozygosity. *Proc Biol Sci*. 274:1895–1903.

Rubenstein DR. 2007b. Stress hormones and sociality: integrating social and environmental stressors. *Proc Biol Sci*. 274:967–975.

Rubenstein DR. 2016. Superb starlings: cooperation and conflict in an unpredictable environment. In: Koenig WD, Dickinson J, editors. *Cooperative breeding in vertebrates: studies of ecology, evolution, and behavior*. Cambridge (UK): Cambridge University Press. p. 181–196.

Seutin G, White BN, Boag PT. 1991. Preservation of avian blood and tissue samples for DNA analysis. *Can J Zool*. 69:82–90.

Shawkey MD, D'Alba L, Xiao M, Schutte M, Buchholz R. 2015. Ontogeny of an iridescent nanostructure composed of hollow melanosomes. *J Morphol*. 276:378–384.

Shuttleworth AC. 1197. Type VIII collagen. *Int J Biochem Cell Biol*. 29:1145–1148.

Simão FA, Waterhouse RM, Ioannidis P, Kriventseva EV, Zdobnov EM. 2015. BUSCO: assessing genome assembly and annotation completeness with single-copy orthologs. *Bioinformatics*. 31:3210–3212.

Smit AFA, Hubley R, Green P. 2013-2015. RepeatMasker Open-4.0. Available from: http://www.repeatmasker.org.

Song L, Florea L, Langmead B. 2014. Lighter: fast and memory-efficient sequencing error correction without counting. *Genome Biol*. 15:509.

Stanke M, Tzvetkova A, Morgenstern B. 2006. AUGUSTUS at EGASP: using EST, protein and genomic alignments for improved gene prediction in the human genome. *Genome Biol*. 7(Suppl 1):S11.1–S11.8.

Sylvester JE, Fischel-Ghodsian N, Mougey EB, O'Brien TW. 2004. Mitochondrial ribosomal proteins: candidate genes for mitochondrial disease. *Genet Med*. 6:73–80.

Team RC. 2019. *R: a language and environment for statistical computing*. Vienna (Austria): R Foundation for Statistical Computing.

Thomas DB, McGraw KJ, Butler MW, Carrano MT, Madden O, James HF. 2014. Ancient origins and multiple appearances of carotenoid-pigmented feathers in birds. *Proc Biol Sci*. 281:20140806.

Toews DPL, Hofmeister NR, Taylor SA. 2017. The evolution and genetics of carotenoid processing in animals. *Trends Genet*. 33:171–182.

Toral GM, Figuerola J, Negro JJ. 2008. Multiple ways to become red: pigment identification in red feathers using spectrometry. *Comp Biochem Physiol B Biochem Mol Biol*. 150:147–152.

Vempati UD, Torraco A, Moraes CT. 2008. Mouse models of oxidative phosphorylation dysfunction and disease. *Methods*. 46:241–247.

Vickrey AI, Bruders R, Kronenberg Z, Mackey E, Bohlender RJ, Maclary ET, Maynez R, Osnborne E, Johnson KJ. 2018. Introgression of regulatory alleles and a missense coding mutation drive plumage pattern diversity in the rock pigeon. *eLife*. 7:e34803.

Weinman LR, Solomon JW, Rubenstein DR. 2015. A comparison of single nucleotide polymorphism and microsatellite markers for analysis of parentage and kinship in a cooperatively breeding bird. *Mol Ecol Resour*. 15:502–511.

Williams TL, Senft SL, Yeo J, Martín-Martínez FJ, Kuzirian AM, Martin CA, DiBona CW, Chen CT, Dinneen SR, Nguyen HT, *et al.* 2019. Dynamic pigmentary and structural coloration within cephalopod chromatophore organs. *Nat Commun*. 10:1004.

Wolf DA 2016. Is reliance on mitochondrial respiration a "Chink in the Armor" of therapy-resistant cancer? *Cancer Cell* 8:788–795.

Xu Y, Zhang XH, Pang YZ. 2013. Association of tyrosinase (TYR) and tyrosinase-related protein 1 (TYRP1) with melanic plumage color in Korean quails (*Coturnix coturnix*). *Asian-Australas J Anim Sci*. 26:1518–1522.

Yodh A, Lin K, Crocker J, Dinsmore A, Verma R, Kaplan P. 2001. Entropically driven self-assembly and interaction in suspension. *Philos Trans R Soc B*. A359:921–937.

Zdarsky E, Favor J, Jackson IJ. 1990. The molecular basis of brown, an old mouse mutation, and of an induced revertant to wild type. *Genetics*. 126:443–449.

Zhu A, Ibrahim JG, Love MI. 2018. Heavy-tailed prior distributions for sequence count data: removing the noise and preserving large differences. *Bioinformatics*. 35:2084–2092.